

# Chemical Bonding in the Ternary Transition Metal Bismuthides $Ti_4TBi_2$ with $T = Cr, Mn, Fe, Co,$ and $Ni$

Ruedi Rytz and Roald Hoffmann\*

Department of Chemistry and Materials Science Center, Cornell University,  
Ithaca, New York 14853-1301

Received September 9, 1998

The electronic structure and chemical bonding in the ternary transition metal bismuthides  $Ti_4TBi_2$  ( $T = Cr, Mn, Fe, Co,$  and  $Ni$ ) is investigated by approximate MO calculations of the extended Hückel tight-binding type. These intermetallic compounds crystallize in a layer structure, repeating sequence  $T-Ti/Bi-T-Ti/Bi$ , stacking along  $c$ ; the late transition metals form linear chains with short  $T-T$  bonds. Other important structural elements are face-sharing chains of  $Ti_4Bi_2$  octahedra and Bi channels. The decrease of the  $T-T$  bond lengths from Cr to Ni is more pronounced than expected from the decrease of the metallic radii alone. The analysis of the electronic structure indicates that this behavior arises from the titanium–titanium and titanium–bismuth interlayer interactions. Diminution of the titanium–titanium interlayer distances as one goes from  $Ti_4CrBi_2$  to  $Ti_4NiBi_2$  is due to  $Ti(d)-Ti(d)$  bonding, which increases with increasing electron filling of the titanium d levels. The titanium–bismuth interactions remain strong along this series, as can also be seen by the constant *intralayer*/titanium–bismuth distances. A distinguishing feature of the title compounds is the channels formed by bismuth atoms. These channels are filled by Bi-centered, essentially unhybridized 6p orbitals forming a 2D net stacking along  $c$  and interacting with each other, stronger in the  $c$  direction than perpendicular to it. The possibility of intercalating electrophilic species into these electron-filled voids is also investigated. abstract

## Introduction

Recently, the ternary transition metal bismuthides  $Ti_4TBi_2$  with  $T = Cr, Mn, Fe, Co,$  and  $Ni$  were prepared and (with the exception of the chromium example) their crystal structures determined by Richter, Jeitschko, Künnen, and Gerdes.<sup>1</sup> The title compounds are isotypic with  $V_4SiSb_2$ , which crystallizes in the tetragonal space group  $I4/mcm$ .<sup>2</sup> A common feature of this structure type is that the elements occupying the atomic position 4a, i.e., Si or  $T$ , form linear chains with short separations along the crystallographic  $c$  axis. As we will see, along the series Cr, Mn, Fe, Co, and Ni the  $T-T$  bond lengths decrease more rapidly than would be expected from the metallic radii. The aim of the present work is to understand the behavior of the  $T-T$  bond lengths in  $Ti_4TBi_2$ , as well as to shed light on the chemical bonding in these appealing compounds.

## Structural Description

The title compounds (we take  $Ti_4FeBi_2$  as a representative example) crystallize in the tetragonal space group  $I4/mcm$  (No. 140) with four formula units per unit cell ( $Z = 4$ ).<sup>1</sup> The asymmetric unit consists of only three atoms, one of each element.

Figure 1a shows a drawing of the iron-containing compound, viewed along the  $c$  axis. The unit cell is outlined, with  $a = b = 1049$  pm and  $c = 493$  pm. Figure 1b presents a view parallel to  $a$  showing a layering, with the repeating sequence  $Fe-Ti/Bi(1)-Fe-Ti/Bi(2)$ . Note the  $Fe-Fe-Fe$  (or  $T-T-T$ ) needle in this lattice. The Fe layer can be viewed as a centered square lattice with the same  $a$  and  $b$  as for the ternary compound.

As may be seen from Figure 1,  $Ti(1,2,3,4)$  and  $Bi(1,2)$  form a distorted octahedron. This octahedron repeats itself along  $c$ , so that the titanium and bismuth atoms actually form columns of face-shared distorted octahedra.

Each bismuth has eight titanium neighbors;  $Ti-Bi$  distances range between 289 and 307 pm. The iron atoms are located at the center of a square antiprism whose square faces are capped by two irons. The relevant distances are  $Fe(1)-Ti(1)$  255 pm ( $8\times$ ) and the short  $Fe(1)-Fe(2)$  contact of 247 pm ( $2\times$ ).

The several interesting features of this compound become apparent. They are as follows: linear chains of iron atoms with relatively short iron–iron distances (247 pm), the chains of face-sharing  $Ti/Bi$  octahedra, and the empty channels formed only by bismuth. While these channels are clearly visible, they are not very wide. The bismuth atoms across the channel are 413 pm apart and belong to the same  $Ti/Bi$  layer. The bismuth atoms belonging to different  $Ti/Bi$  layers are at a distance of 382 pm.

## Where are the Electrons?

$Ti_4FeBi_2$  contains the first-row transition metals Ti and Fe and the Group 15 semimetallic element Bi. In order to get a preliminary, though crude, feeling for the charge distribution, consider the formal oxidation numbers of the atoms in question. We assign  $-3$  to bismuth, based on the apparent absence of  $Bi-Bi$  bonds (the shortest  $Bi-Bi$  separation is 382 pm) and the high electronegativity of Bi *vis-à-vis* the other elements in the compound. If we further assume, just as a starting point, that titanium—the most electropositive atom—contributes all of its valence electrons to iron and bismuth, we come to  $(Ti^{4+})_4Fe^{10-}(Bi^{3-})_2$ . An oxidation state of  $+4$  for titanium is not uncommon, but the highly reduced iron is, to put it mildly, rather unusual.

The electron-counting scheme as described above excludes the possibility of titanium–titanium and iron–iron interactions.

\* Corresponding author. E-mail: rh34@cornell.edu.

(1) Richter, C. G.; Jeitschko, W.; Künnen, B.; Gerdes, M. H. *J. Solid State Chem.* **1997**, *133*, 400.

(2) Wollesen, P.; Jeitschko, W. *J. Alloys Compd.* **1996**, *243*, 67.

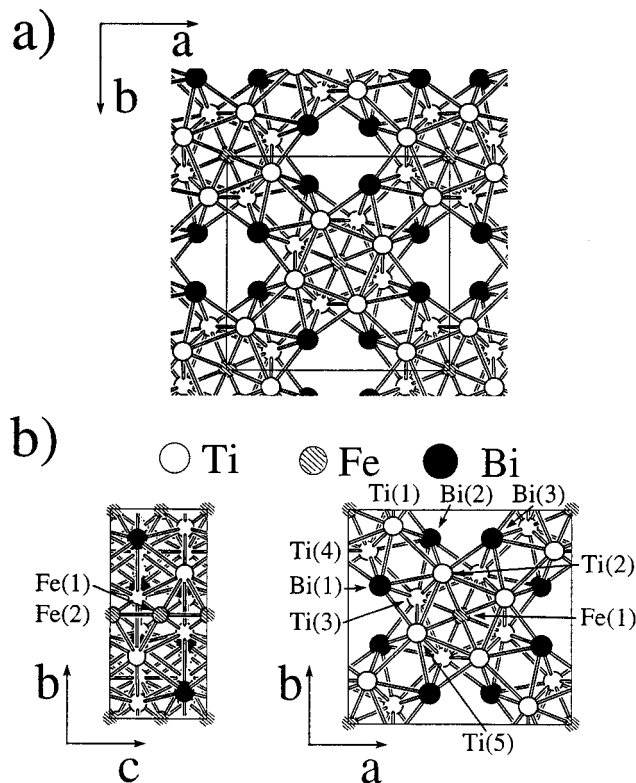


**Figure 1.** Structure of the tetragonal  $\text{Ti}_4\text{FeBi}_2$  compound. (a) Extended structure viewed along  $c$  where the unit cell is framed. (b) Left: The unit cell viewed along  $a$ . Right: The unit cell viewed along  $c$ . (All atoms of the same type are related by symmetry. The atom numbering is for convenience only.)

However, the shortest Fe–Fe and Ti–Ti distances in this compound are 247 and 299 pm, respectively; the former is certainly short. Richter *et al.* suggest a charge assignment ( $\text{Ti}^{3+}$ ) $_4\text{Fe}^{6-}(\text{Bi}^{3-})_2$  in order to allow Fe–Fe and Ti–Ti interactions.<sup>1</sup>

We do not wish to dwell on these electron assignments, for they are to a great extent a formality. Moreover, a description of the chemical bonding in intermetallic phases is difficult in terms of simple valence rules,<sup>3</sup> which are otherwise extremely useful.<sup>4–6</sup> A more detailed understanding can be achieved by quantum chemical calculations. In the following we present the results obtained from extended Hückel tight-binding calculations<sup>7,8</sup> (details of the computations are given in the Appendix) of the electronic structure of this interesting group of materials.

### The Electronic Structure of $\text{Ti}_4\text{FeBi}_2$

For  $\text{Ti}_4\text{FeBi}_2$  the charges computed from a Mulliken population analysis<sup>9</sup> are 0.63,  $-2.41$ , and  $-0.05$  for titanium, iron, and bismuth, respectively. As far as the signs are concerned, the computed net charges reflect the trends we have obtained from the simple electron-counting procedure described in the previous section. However, bismuth is almost neutral, suggesting that this element is more involved in covalent than ionic bonding

toward its eight titanium neighbors. We will return to this point later in the course of a crystal orbital overlap population (COOP) analysis.<sup>8,10</sup>

In Figure 2 we show the density-of-states (DOS) contributions from the three elements in the energy region from  $-20$  to  $10$  eV. The solid line represents the total DOS, and the hatched areas are the respective contributions of titanium (left panel), iron (middle panel), and bismuth (right panel). The Fermi level ( $E_f$ , dotted horizontal line) lies at  $-6.4$  eV. Experimentally  $\text{Ti}_4\text{FeBi}_2$  was found to be metallic by electrical resistivity measurements on sintered, porous samples of the material,<sup>1</sup> consistent with  $E_f$  coming in a region of high DOS. In the range from  $-14.6$  to  $-11.3$  eV there are no states.

Just below this region we find the bismuth 6s orbitals, which remain relatively well localized at about their valence orbital ionization energy  $H_{6s6s} = -15.19$  eV. There is some slight broadening of the Bi(6s) states caused by Ti(4s)–Bi(6s) interactions.

The Bi(6p) levels spread from  $-11.3$  all the way up to  $10$  eV, with a significant portion localized in the energy region from  $-11.3$  eV to  $E_f$ . There is little Bi s–p mixing, a situation typical of lower Group 15 elements.<sup>11,12</sup>

The iron projection shows that the sharp peak just above the energy gap, at about  $-9.5$  eV, can be ascribed to Fe(3d) orbitals. Occupation of these orbitals leads to a large negative charge ( $-2.41$ ) on the iron centers as calculated from a Mulliken population analysis. The Fe(3d) orbitals accommodate a total of 8.76 electrons. The charge accumulation in the Fe(3d) is related to the contraction of these orbitals, which leads to a (I) spatial and (II) energetic localization of these levels: First, the Fe(3d) are strongly contracted, as can be seen from the calculated orbital radius  $r_n(3d) = 43$  pm (eqs 13, 14a, and 14b in ref 13). Electrons in contracted orbitals do not contribute much to covalent chemical bonding for they remain *spatially* localized, which is reflected in a high Mulliken population, if those states come below the Fermi level. Second, the value of  $r_n(3d) = 43$  pm has to be compared with the shortest iron–iron and iron–titanium distances of 247 and 255 pm, respectively. This suggests that Fe(3d) orbitals overlap less with neighboring atomic orbitals than, e.g., Fe(4s) and Fe(4p) with orbital radii of 111 pm each. Moreover, because of the square antiprismatic coordination around Fe,  $3(d_{x^2-y^2}, d_{xy}, d_{z^2})$  interact only weakly with the titanium orbitals. As the interaction energy of two atomic orbitals depends on their spatial overlap, it is no surprise that the Fe(3d) states remain *energetically* localized at about their valence orbital ionization energy of  $H_{3d3d} = -9.2$  eV.

The Fermi level region is dominated by titanium-based states, mainly Ti(3d).

### Where are the Bonds?

In Figure 3 we present the crystal orbital overlap population (COOP) curves (solid lines) for all relevant atom–atom interactions in  $\text{Ti}_4\text{FeBi}_2$ . The atoms which give rise to the respective COOP curve (the numbering is in Figure 1) and the corresponding bond lengths are given as insets. The dotted line in each graph is the integration of the COOP curve; the Fermi level ( $-6.4$  eV) is marked by a dotted line running horizontally. A positive (negative) value of the COOP at a given energy means that the collective interaction of the atomic orbitals at

(3) Nesper, R. *Angew. Chem., Int. Ed. Engl.* **1991**, *30*, 789.

(4) Jørgensen, C. K. *Oxidation Numbers and Oxidation States*; Springer-Verlag: Berlin; Heidelberg; New York, 1969.

(5) Burdett, J. K. *Molecular Shapes*; John Wiley & Sons: New York; Chichester; Brisbane; Toronto; Singapore, 1980.

(6) Calzaferri, G. *J. Chem. Educ.* **1999**, *76*, 362.

(7) Hoffmann, R. *J. Chem. Phys.* **1963**, *39*, 1397.

(8) Hoffmann, R. *A Chemist's View of Bonding in Extended Structures*; VCH Verlagsgesellschaft: Weinheim; New York, 1988.

(9) Mulliken, R. S. *J. Chem. Phys.* **1955**, *23*, 1833.

(10) Hughbanks, T.; Hoffmann, R. *J. Am. Chem. Soc.* **1983**, *105*, 3528.

(11) Seo, D.-K.; Hoffmann, R., submitted for publication.

(12) Papoian, G.; Hoffmann, R., in preparation.

(13) Calzaferri, G.; Forss, L.; Kamber, I. *J. Phys. Chem.* **1989**, *93*, 5366.

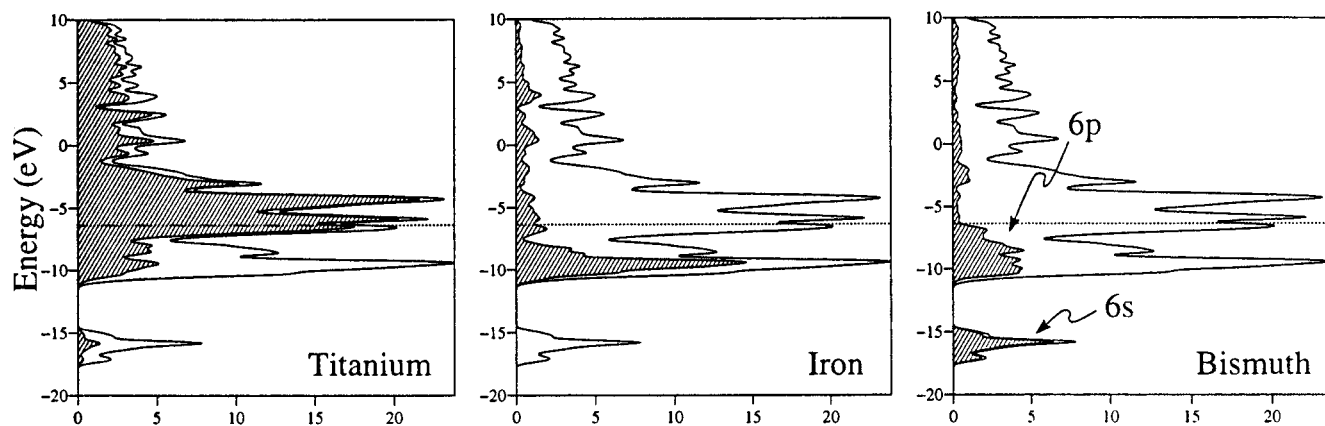


**Figure 2.** Density of states (DOS) of  $\text{Ti}_4\text{FeBi}_2$  in the energy region from  $-20$  eV to  $10$  eV. The dotted horizontal line indicates the Fermi level at  $-6.4$  eV. The solid lines represent the total DOS. The hatched regions show the DOS contributions from titanium (left panel), iron (middle panel), and bismuth (right panel) where the contributions of the s, p, and d orbitals (Ti, Fe), and s, p orbitals (Bi) are added up.

both atoms is bonding (antibonding), as measured by a Mulliken overlap population. In order to determine the overall interaction of two atoms at a given distance, bonding and antibonding contributions are integrated up to the Fermi level.

We distinguish three cases: The integration of the COOP curve is maximal (I) below, (II) above, or (III) just at the Fermi level. In case III, the structure obviously maximizes bonding. In case I there are too many and in case II insufficient electrons for optimal bonding between the atoms considered. On this basis, we assign the COOP curves in Figure 3 to the three categories as follows: (I) a, b (Fe–Fe and Bi–Bi); (II) c–e (all Ti–Ti); (III) f–i (Fe–Ti and all Bi–Ti). It is impossible to directly compare the magnitudes of the various COOP curves for different bond types (e.g., Bi–Bi with Fe–Fe).<sup>14</sup> However, if we assume that “nature” assembles the compound so as to optimize the important (that is, the strongest) bonds for a given electron count, we would argue that chemical bonding can be understood as a compromise between the structure-determining interactions of type III (which are optimized) and the apparently less important, perhaps “packing-governed,” interactions of types I and II. In the following, we briefly discuss the individual COOP curves in  $\text{Ti}_4\text{FeBi}_2$  in Figure 3.

(a) The iron–iron interaction at the short distance of  $247$  pm is bonding, even though the maximal-bonding electron filling is far below the Fermi level. The Fe(3d) block is largely filled: the bonding derives from occupation of the bonding part of the Fe(4s) and Fe(4p) bands, and Fe–Fe interactions mixing s, p, into the d block. To evaluate the integrated Fe–Fe COOP one needs some calibration. Bona fide unsupported Fe–Fe single and double bonds are rare. A theoretical estimate is obtained by approaching two  $\cdot\text{FeH}_5^{4-}$  fragments (isolobal to  $\cdot\text{CH}_3^{15,16}$ ) yielding an Fe–Fe single bond, and two  $:\text{FeH}_4^{4-}$  fragments (isolobal to  $:\text{CH}_2$ ) yielding an Fe=Fe double bond. From Figure 4 we see that the integrated Fe–Fe COOP of  $0.2$  found in  $\text{Ti}_4\text{FeBi}_2$  is roughly half of the reduced overlap population expected for an Fe–Fe single bond.

(b) The bismuth–bismuth interaction for the shortest Bi–Bi distance of  $382$  pm is small and essentially nonbonding, as can be seen by the almost vanishing integrated COOP at the Fermi level. The fact that the overall interaction is small is no surprise

if we bear in mind that the covalent radius of bismuth is  $153$  pm.<sup>17</sup> Below  $-15$  eV we find a Bi(s)–Bi(s) bonding region, immediately followed by the Bi(s)–Bi(s) antibonding one. The same “S-shape pattern” is observed for the Bi(p) orbitals starting above the band gap at  $-11.3$  eV. Such “S-shape patterns” below  $E_f$  are the result of a filled, pretty much non-interacting (with other orbitals) bands (cf. ref 8, pp 42 ff). The situation is typical of two-orbital-four-electron interactions; this is where a steric repulsion shows up. The other two short bismuth–bismuth interactions (not shown in Figure 3) at distances of  $411$  and  $413$  pm for the bismuth atoms at the apices of the titanium–bismuth octahedra and across the channels, respectively, are weak and nonbonding, too.

(c–e) The titanium–titanium interactions are bonding, although all of the Ti–Ti bonds are somewhat short of electrons, relative to the electron filling that would yield maximal bonding. The COOP for the shortest titanium–titanium contact of  $299$  pm (which connects two corners of neighboring squares that form the titanium antiprism) is given in panel c. The titanium squares are twisted against each other by  $44.5^\circ$ , so we find other, only slightly longer ( $301$  pm), corner-connecting titanium–titanium bonds, e.g., Ti(3)–Ti(5). The Ti(3)–Ti(5) COOP curve in the relevant energy region from  $-18$  to  $-5$  eV is almost identical with the curve in panel c and therefore not given here. It is clear that the Ti(2)–Ti(3) bond is much stronger than Ti(2)–Ti(5) and Ti(2)–Ti(1). The difference in bond energy is probably even greater than the integrated COOP curves suggest and is caused by d–d interaction.

(f) The electron filling is optimal for the iron–titanium interaction, indicating strong Fe–Ti bonding.

(g–i) Again we find an optimal electron count for all of the three different bismuth–titanium bonds. The contributions to the COOP curves at  $-15$  eV are of the Ti(s,p,d)–Bi(s) type, with Ti(s)–Bi(s) dominant. The second bonding contribution just after the gap is of the Ti(s,p,d)–Bi(p) type.

In the above we have argued for Bi–Ti interactions being most important in determining the structure of these phases. At the same time there definitely is linear chain transition metal–metal bonding.

In the next section we will use the preceding results in order to understand the decrease in the lattice size along  $c$  of these phases upon going from Cr to Ni.

(14) Albright, T. A.; Burdett, J. K.; Whangbo, M.-H. *Orbital Interactions in Chemistry*; John Wiley & Sons: New York; Chichester; Brisbane; Toronto; Singapore, 1998; p 23.

(15) Hoffmann, R. *Angew. Chem., Int. Ed. Engl.* **1982**, *21*, 711.

(16) Elian, M.; Chen, M. M. L.; Mingos, D. M. P.; Hoffmann, R. *Inorg. Chem.* **1976**, *15*, 1148.

(17) Pauling, L. *Nature of the Chemical Bond*; Cornell University Press: Ithaca, NY, 1944.

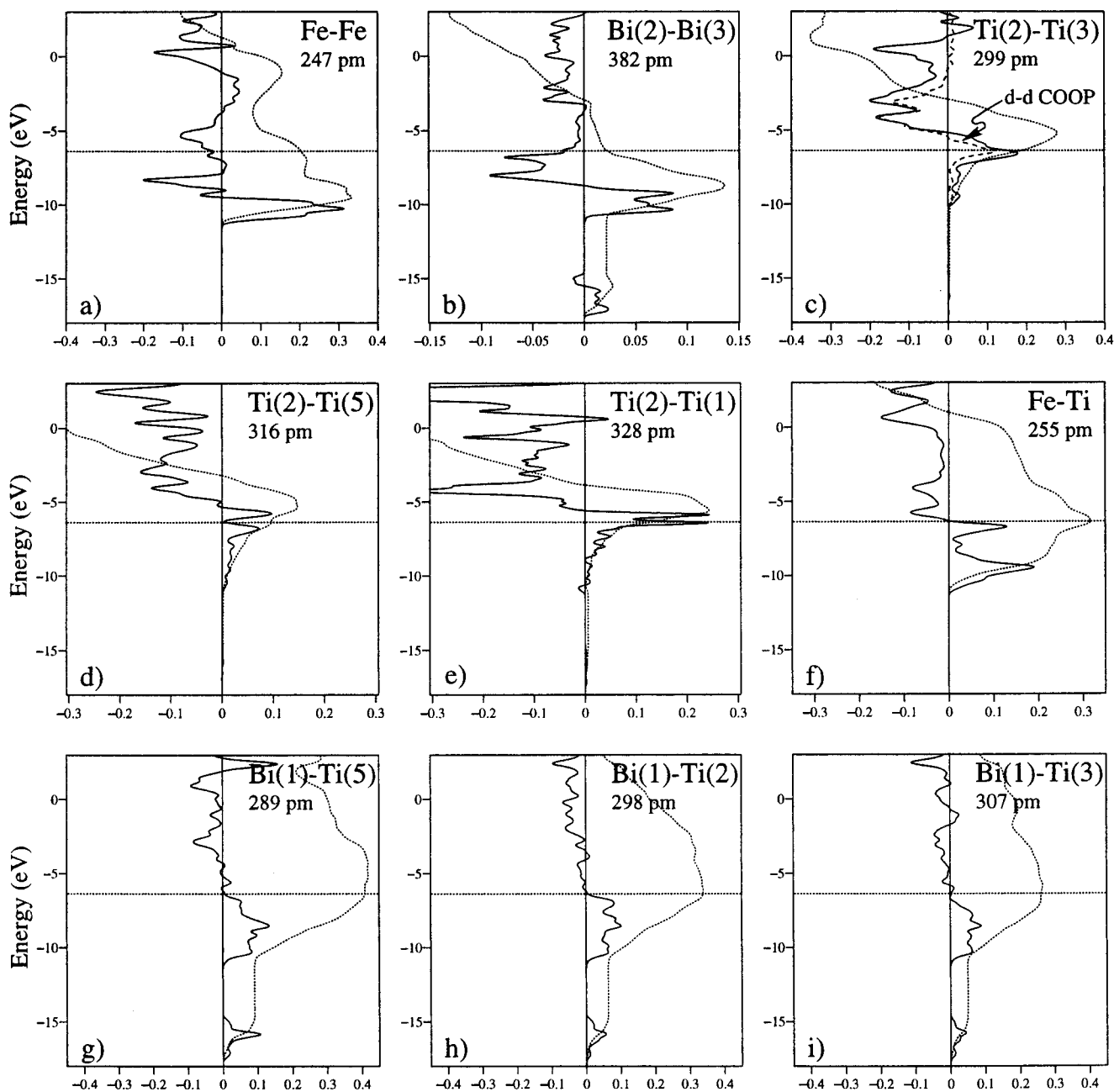


**Figure 3.** Crystal orbital overlap population (COOP) curves for all relevant atom–atom interactions in  $\text{Ti}_4\text{FeBi}_2$ . The atoms which give rise to the respective COOP and the corresponding bond lengths are given as insets. The solid lines give the COOP curves while the dotted lines represent their integrations. The dotted horizontal line indicates the Fermi level at  $-6.4$  eV.

### The Series $\text{Ti}_4T\text{Bi}_2$ , with $T = \text{Cr, Mn, Fe, Co, and Ni}$

In Figure 5 we compare the lattice constants  $c$  for  $\text{Ti}_4T\text{Bi}_2$  where  $T = \text{Cr, Mn, Fe, Co, and Ni}$  (diamonds in graph) with the metallic radii for coordination number 12 (circles).<sup>18</sup> As the unit cell size along  $c$  is spanned by two  $T$ – $T$  bonds, the quadrupled metallic radii of  $T$  are plotted. Both the lattice constants and the metallic radii decrease as we go from Cr to Mn. However, two differences should be noted: First, there is no increase in the lattice constant on passing from Mn to Fe. Second, the decrease is more pronounced for the lattice constant than for the metallic radii. The difference in  $c$  between chromium and nickel is 25 pm, while the difference in the metallic

radii is 14 pm or roughly 56% of the aforementioned value. The trend is significant, though not huge, and can be understood as due to an interplay of the following two factors.

(I) The increase of the Fermi level from  $-6.4$  eV (Mn) to  $-6.2$  eV (Ni) leads to an occupation of previously empty Ti(3d) orbitals and thereby to a strengthening of the titanium–titanium bonds which connect neighboring Ti/Bi layers (Figure 3c). As they become stronger, these bonds contract, decreasing the unit cell length along  $c$ .

On going to the right in the periodic table from one late transition metal to the next we add four electrons per unit cell. A high percentage of these electrons enter titanium d levels that dominate the electronic character of these phases at  $E_f$ . As the occupation of Ti(4s) and Ti(4p) orbitals remains practically unchanged, it is possible to monitor the buildup of electron density in Ti(3d) by following the titanium net charge decrease

(18) Pearson, W. B. *The Crystal Chemistry and Physics of Metals and Alloys*; John Wiley & Sons: New York; Chichester; Brisbane; Toronto; Singapore, 1971.

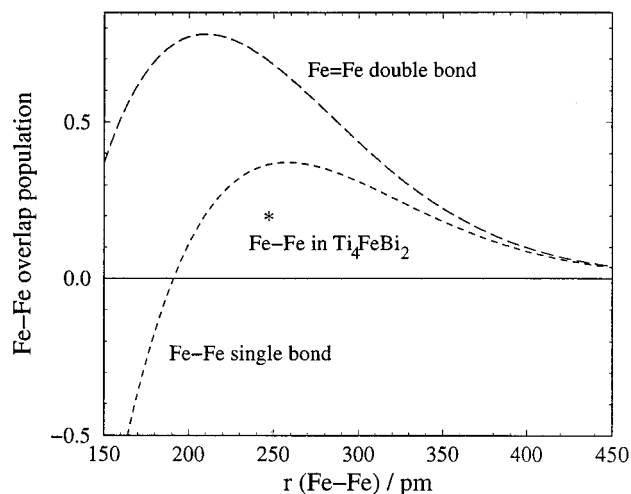


**Figure 4.** Reduced overlap population between two Fe atoms vs Fe-Fe distance for a typical Fe-Fe single bond (in  $H_5Fe-FeH_5^{8-}$ ) and Fe=Fe double bond (in  $H_4Fe=FeH_4^{8-}$ ) compared with the Fe-Fe bond in  $Ti_4FeBi_2$ .

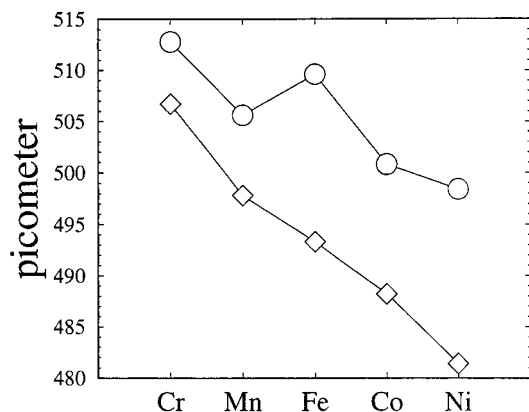


**Figure 5.** Comparison of the lattice parameter along  $c$  for  $Ti_4Tb_i_2$  where  $T = Cr, Mn, Fe, Co,$  and  $Ni$  (diamonds,  $\diamond$ ) with the quadrupled metallic radii for coordination number 12 given in ref 18 (circles,  $\circ$ ).

from 0.77 in  $Ti_4MnBi_2$  to 0.27 in  $Ti_4NiBi_2$ . Additional d-d interaction is mainly responsible for the decrease of the interlayer  $Ti(2)-Ti(3)$  bond lengths from 301 (Mn) to 297 pm (Ni). The same holds for the bonds of the  $Ti(5)-Ti(3)$  type, which decrease in length from 303 (Mn) to 297 pm (Ni). As shown in Figure 5, the shortening of these bonds cannot be explained only with the decrease of the metallic radii of  $T$  along this series. As a matter of fact, the eight manganese-titanium bonds are 257 pm and thus even slightly shorter than the corresponding nickel-titanium ones, which are 258 pm. To get a clearer picture of the  $Ti(2)-Ti(3)$  bonds that are subject to contraction we have drawn in Figure 6 a side view of the columns of distorted  $Ti_4Bi_2$  octahedra. These bonds form the short edges  $e$  of the octahedra. The bond lengths  $e$  of the whole series are compiled in Table 1.

(II) The shortening of  $Ti-Bi$  bonds across the layer which we have labeled  $b$  in Figure 6 also contributes to the contraction of the unit cell along  $c$ . On going from Mn to Ni we find that  $b$  decreases, while  $a$  almost remains constant (Table 1). This can be understood as follows: The four titanium atoms  $Ti(1,2,3,4)$  form the rectangular basal plane of a distorted  $Ti_4Bi_2$  octahedron. We have previously pointed out that titanium-bismuth bonding is expected to be strong. Maximal  $Bi-Ti$  bonding of the two apical bismuths with the four titaniums is presumably obtained if all eight titanium-bismuth bond

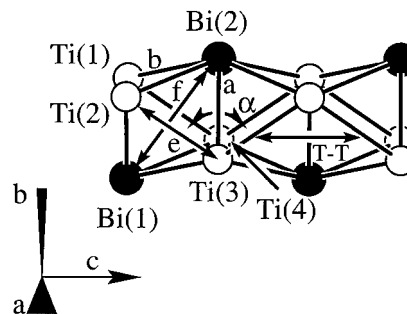


**Figure 6.** Side view of the columns which consist of face-sharing  $Ti_4Bi_2$  octahedra. The atoms are labeled as in Figure 1b.

**Table 1.** Experimental Bond Lengths, Bond Angles, and Computed Net Charges for the Ternary Transition Metal Bismuthides  $Ti_4Tb_i_2$ <sup>a</sup>

	Mn	Fe	Co	Ni
$a \equiv d(Ti(3)-Bi(2))$ (pm)	298	298	299	299
$b \equiv d(Ti(2)-Bi(2))$ (pm)	308	307	305	301
$a/b$	0.97	0.97	0.98	0.99
$e \equiv d(Ti(2)-Ti(3))$ (pm)	301	299	298	297
$f \equiv d(Bi(1)-Bi(2))$ (pm)	413	411	409	407
$\alpha_{ideal} \equiv 2 \arctan(f/e)$ (deg)	107.7	107.8	107.9	107.8
$\alpha_{exp}$ (deg)	111.3	111.1	110.2	108.4
$i \equiv d(Ti(2)-Ti(1))$ (pm)	326	328	329	325
$k \equiv d(Ti(2)-Bi(3))$ (pm)	289	289	290	290
computed charge on $Ti^b$	0.77	0.62	0.46	0.27

<sup>a</sup> For the chromium compound, only the cell parameters were determined in ref 1. <sup>b</sup> Extended Hückel calculation.

lengths are equal. This would point to equal length  $a$  and  $b$  bonds; indeed we find that the ratio  $a/b$  approaches the ideal value of 1.

Yet another way of describing the drive to decrease the strain in the titanium-bismuth columns (and taking into account the simultaneous shortening of  $e$ ) goes as follows: Given the length of the short edge of the titanium base  $e$  and the distance of the capping bismuth atoms  $f$ , the angle between two neighboring basal planes for an unstrained  $Ti_4Bi_2$  column is  $\alpha_{ideal} = 2 \arctan(f/e)$ . The experimental value  $\alpha_{exp}$  approaches  $\alpha_{ideal}$  along the series.

The unit cell size along  $a$  and  $b$  changes little from Cr to Ni. The distance between two neighboring late transition metal centers within the  $T$  layers is  $r = (2^{1/2}l/2)$ , where  $l$  is  $|a|$  or  $|b|$ . While the other bond lengths within the layer change with  $r$ ,  $Ti(2)-Bi(3)$  remains almost constant (Table 1). This once again provides evidence for strong titanium-bismuth bonding in the  $Ti_4Tb_i_2$  compounds.

By analogy with our results for the ternary transition metal bismuthides, we speculate that the short Si-Si distance of 235 pm (the same as in the diamond modification of silicon) in the isotopic  $V_4SiSb_2$  can be attributed to strong and optimized vanadium-antimony interactions.

### The Bismuth Channels

A distinguishing feature of the title compounds, apparent in Figure 1a, is that of channels formed by bismuth atoms. Richter *et al.* reasonably assume a filling of these channels with nonbonding electrons, i.e., with bismuth lone pairs.<sup>1</sup> "Stereochemically active" lone pairs are frequently observed in the chemistry of  $Bi(III)$  and are known not only to influence its coordination sphere but also to give rise to interesting electronic properties. In  $CH_3BiI_2$ , for example, Bi is square-pyramidally coordinated, four iodines forming the slightly distorted basal

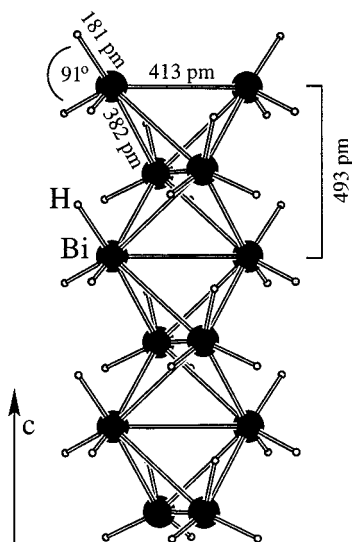


**Figure 7.** Side view of a bismuth model channel assembled of one-dimensional chains of  $C_{3v}$   $\text{BiH}_3$  molecules. The propagation of the channel is along the  $c$  direction.

plane and the methyl group in the apical site.<sup>19</sup> This less than maximally symmetrical local geometry of bismuth can be explained with a “stereochemically active” lone pair that completes the expected “octahedral” coordination. For  $\text{CH}_3\text{BiI}_2$  the two-orbital-four-electron interaction between lone pairs of neighboring bismuth atoms was found to be slightly repulsive.<sup>19</sup> There are also compounds such as  $\text{Cs}_8\text{Bi}_4(\text{P}_2\text{Se}_6)$  which feature bismuth–bismuth contacts as short as 353 pm,<sup>20</sup> which have sometimes been interpreted in terms of unexpected “lone-pair–lone-pair attractions”. We think (as McCarthy *et al.*<sup>20</sup> note) that—as for lead compounds, e.g.,  $\text{PbO}$ —it is possible to understand short  $\text{Pb–Pb}$  (or  $\text{Bi–Bi}$ ) distances in terms of donor–acceptor interactions (between  $\text{Pb}$  lone pairs and  $\text{Pb–O } \sigma^*$  levels, in  $\text{PbO}$ , for example<sup>21</sup>). In  $\text{RhBi}_4$ , finally, bismuth lone pairs are reported to form insulating hyperbolic layers which separate metallic rhodium–bismuth nets.<sup>22</sup>

As a starting point for an analysis, we model such a bismuth channel in a molecular way, as a one-dimensional chain of  $C_{3v}$   $\text{BiH}_3$  molecules, drawn in Figure 7. The drawn-in bismuth–bismuth “bonds” are not meant to imply actual bonding but merely emphasize their geometrical interrelationship being located in the corners of imperfect edge-sharing tetrahedra. In Figure 8 contour plots at two different positions perpendicular to  $c$  of the highest occupied crystal orbital (CO) at  $\Gamma$  of such a 1D  ${}^\infty[\text{BiH}_3]_4$  chain are shown. In the upper part of the drawing we look down the channel parallel to  $c$ , and in the lower part a side view parallel to  $b$  is presented. The dashed arrows in the lower part of the figure indicate the extension of the channels to infinity along this direction. The lone-pair character of this crystal orbital is apparent: Bismuth 6p and 6s orbitals mix so that lobes pointing toward the center of the channel form. These lobes stack along  $c$  and interact in a bonding way across and in an antibonding way along the channel. As there are four such lone pairs per unit cell, we also expect four bismuth lone-pair-derived energy bands.

In Figure 9, we see the band structure of this 1D  ${}^\infty[\text{BiH}_3]_4$  chain. The direction from  $\Gamma$  to  $Z$  corresponds to the  $c$  axis of the real-space unit cell; this is the direction of the propagation of the 1D chain. The Fermi level at  $-7.7$  eV is indicated by a dotted line. The crystal orbitals giving rise to the four energy bands (1–4) immediately below  $E_f$  are the sought-after bismuth “lone pairs”. In the following section we briefly discuss the way these bands run from  $\Gamma$  to  $Z$  and what we can learn from it about the magnitude of the lone-pair interaction along and across the channel.

The crystal orbital belonging to band 1 at  $\Gamma$  is the in-phase combination of all lone pairs across and along the  ${}^\infty[\text{BiH}_3]_4$  chain and consequently has the lowest energy of all of the four bands in question ( $-12.5$  eV). As we go to  $Z$ , antibonding lone-pair interactions between neighboring unit cells show up; the band increases in energy and “runs up”.

The wave function of band 4 at  $\Gamma$  consists of bismuth lone pairs which are in-phase (therefore bonding) across the channel but antibonding between orbital lobes of neighboring  $ab$  planes (Figure 8). At  $Z$ , however, half of these interactions (the ones between neighboring unit cells) become bonding. The energy of this band drops; the band as a whole “runs down”. At this symmetry point of the Brillouin zone, the crystal orbitals of bands 1 and 4 are related by a  $4_2$  screw-rotation and are thus degenerate. (The same must hold for all bands at  $Z$ .)<sup>23</sup> The energy splitting of bands 4 and 1 at  $\Gamma$  is 4.8 eV (or 1.2 eV per bismuth lone pair), which is a good measure for the bismuth–lone-pair interaction *along* the channel.

The band labeled 2,3 is doubly degenerate throughout the Brillouin zone. The corresponding crystal orbitals feature out-of-phase combinations of bismuth lone pairs across the channel. As this interaction is restricted to every *next but one*  $ab$  plane, the energy of these crystal orbitals depends only little on  $k$ ; the band is almost flat. The energy difference between band 2,3 and the lone pair in a  $\text{BiH}_3$  molecule is roughly 0.8 eV (or 0.4 eV per bismuth lone pair), which is a measure for the destabilization arising from (antibonding) bismuth–lone-pair interaction across the channel. As the corresponding bonding interaction is somewhat smaller in magnitude, we conclude that for the given geometry the lone-pair interaction across the channel is smaller than the one encountered between lone pairs lying in neighboring  $ab$  planes. This is so even though in the former case the orbital lobes point directly toward each other. The interaction energies involved are certainly larger than van der Waals type ones and occur at longer bismuth–bismuth contacts than the closed-shell  $\text{Bi–Bi}$  interaction distances (350–380 pm) recently reviewed by Pyykkö.<sup>24</sup>

We now return to the full 3D electronic structure of  $\text{Ti}_4\text{FeBi}_2$ . In Figure 10 we show contour plots of the most bonding (a) and the most antibonding (b) crystal orbitals at  $\Gamma$  which show bismuth–lone-pair character. Even though there are  $\text{Fe}(d_{z^2})$  (in a) and  $\text{Ti}(d_{x^2-y^2})$  (in b) admixtures to these COs, the bismuth contributions are 67% and 45%, as determined from the charge matrix elements, and the orbital energies are  $-10.4$  and  $-6.6$  eV, respectively. From the nodal character of the COs *in* the channels, we find a correspondence of the crystal orbitals of the 1D model chain with the ones for the full structure: At  $\Gamma$  they are CO of band 1 in Figure 9  $\leftrightarrow$  CO plotted in Figure 10a, and CO of band 4 in Figure 9  $\leftrightarrow$  CO plotted in Figure 10b.

In the case of the model channel, interaction of the bismuth and hydrogen orbitals gives rise to significant  $\text{Bi } s\text{–}p$  mixing,

(19) Wang, S.; Mitzi, D. B.; Landrum, G. A.; Genin, H.; Hoffmann, R. *J. Am. Chem. Soc.* **1997**, *119*, 724.

(20) McCarthy, T. J.; Hogan, T.; Kannewurf, C. R.; Kanatzidis, M. G. *Chem. Mater.* **1994**, *6*, 1072.

(21) Trinquier, G.; Hoffmann, R. *J. Phys. Chem.* **1984**, *88* (26), 6696.

(22) Grin, Y.; Wedig, U.; von Schnering, H. G. *Angew. Chem., Int. Ed. Engl.* **1995**, *34* (11), 1204.

(23) Bradley, C. J.; Cracknell, A. P. *The Mathematical Theory of Symmetry in Solids*; Oxford University Press: Oxford, New York, 1972.

(24) Pyykkö, P. *Chem. Rev.* **1997**, *97*, 597.

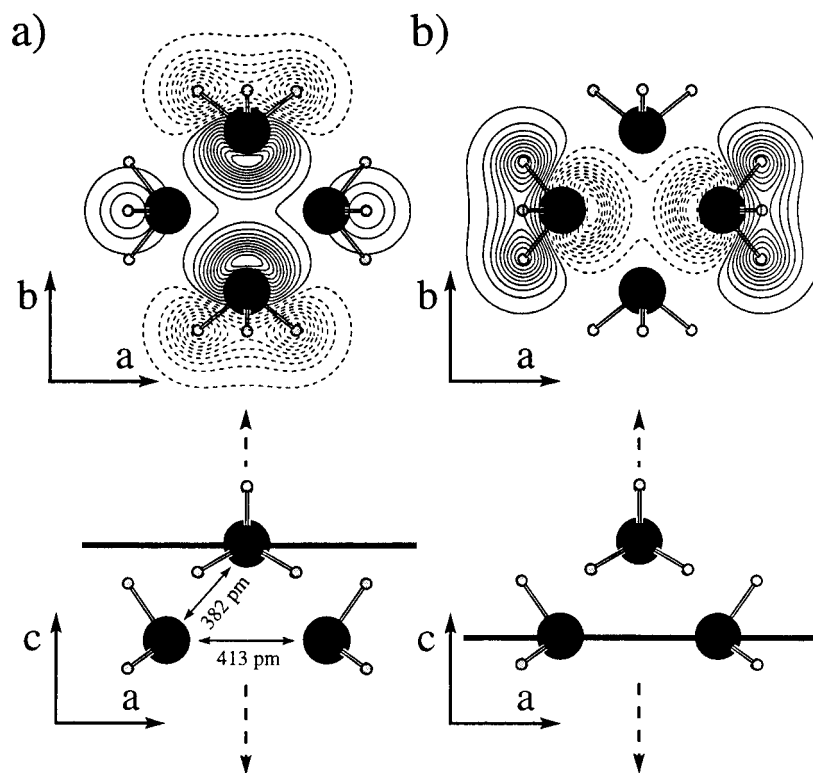


**Figure 8.** Contour plots at two different positions along  $c$  of the highest occupied crystal orbital at  $\Gamma$  of a one-dimensional  ${}^1_{\infty}[\text{BiH}_3]_4$  chain. In the upper part of the figure we look down the channel parallel to  $c$ ; in the lower part a side view parallel to  $b$  is presented. The bold lines give the positions perpendicular to  $c$  where the contours were taken. The dashed arrows indicate the channel axis. Positive phases are drawn with solid lines, negative phases with dashed lines.

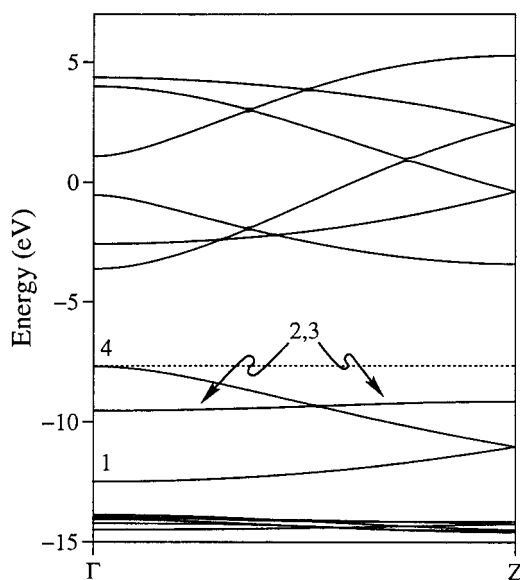


**Figure 9.** Band structure for a one-dimensional  ${}^1_{\infty}[\text{BiH}_3]_4$  model chain. The dotted line indicates the Fermi level  $E_f$ . The four energy bands 1–4 immediately below  $E_f$  are the bismuth “lone pairs”.

which results in lone pairs pointing to the center of the channel. In the ternary bismuthides the Bi–Fe distance is long (424 pm), and the titanium atoms are left as the only possible bismuth neighbors to induce  $s$ – $p$  mixing on this element. However, all titanium orbitals are energetically at least 8.9 eV apart from Bi(6s), which makes them ineffective at inducing hybridization. Hence, our search for bismuth lone pairs pointing into the channels ends by finding a 2D net of bismuth-centered, essentially unhybridized 6p orbitals, stacking along  $c$ , and interacting

with each other, stronger in the  $c$  direction than perpendicular to it. Overlap of the 6p orbitals within the  $\text{Ti}_4\text{Bi}_2$  octahedra provides electronic communication between bismuth channels in the  $a$  and  $b$  directions.

How can we compare the strengths of the bismuth-lone-pair interactions in the model chain versus the full 3D electronic structure? We note that the energy difference at  $\Gamma$  of the two crystal orbitals in question is 4.8 eV (1.2 eV per lone pair) in the model chain and 3.8 eV (0.48 eV per “lone-pair”, i.e., unhybridized Bi(6p) orbital) in  $\text{Ti}_4\text{FeBi}_2$ , which suggests weaker interaction per bismuth atom in the latter case. It is probable that the degree of “lone-pair” hybridization is responsible for this difference.

#### Hypothetical Intercalation of Atoms into the Bismuth Channels

Whenever there are electron-lined voids in a solid, there comes to mind the opportunity of filling them, especially by electrophilic species. Examples of such chemical utility are zeolites<sup>25</sup> and lithium- or alkali-metal-intercalated materials such as some batteries,<sup>26</sup> as well as materials that exhibit ionic conductivity.<sup>27</sup>

The channels in  $\text{Ti}_4\text{TbBi}_2$  are formed by (slightly distorted) edge-sharing bismuth tetrahedra centered in the iron layers. The space in these channels is rather narrow, but the distance from the center to the corners of an imperfect bismuth tetrahedron is still 241 pm, room enough for  $\text{H}^+$  and the alkali-metal cations

(25) Calzafarri, G.; Gfeller, N. *J. Phys. Chem.* **1992**, 96 (8), 3428.

(26) Linden, D., Ed. *Handbook of Batteries and Fuel Cells*; McGraw-Hill: New York, 1984.

(27) Takahashi, T., Ed. *High Conductivity Solid Ionic Conductors: Recent Trends and Applications*; World Scientific Publishing Co.: Singapore; Teaneck, NJ, 1989.

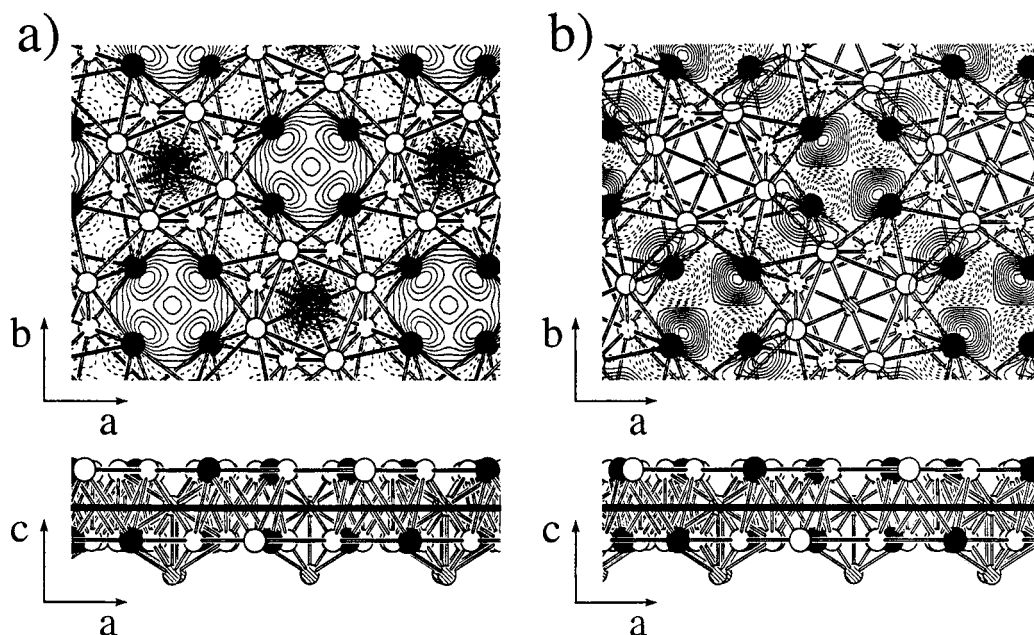


**Figure 10.** Contour plots of the most bonding (a) and most antibonding (b) crystal orbitals at  $\Gamma$  of  $\text{Ti}_4\text{FeBi}_2$  which show “bismuth-lone-pair” character. The corresponding energies are  $-10.4$  and  $-6.6$  eV, respectively. In the upper part of the figure we look down the  $c$  axis; in the lower part a side view parallel to  $b$  is presented. The bold lines indicate that the contours were taken in the iron layer perpendicular to  $c$ . Positive phases are drawn with solid lines, negative phases with dashed lines.

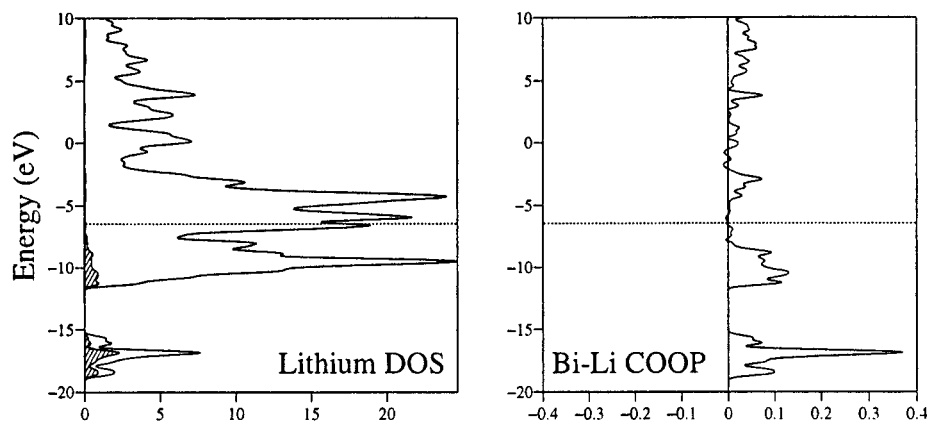


**Figure 11.** Left: Density of states (DOS) of the hypothetical intercalation compound  $\text{Li}^+_x\text{-Ti}_4\text{FeBi}_2$  ( $x = 1$ ) in the energy region from  $-20$  eV to  $10$  eV. The dotted horizontal line indicates the Fermi level at  $-6.5$  eV. The hatched region shows the lithium contribution. Right: Crystal orbital overlap population (COOP) for the interaction of bismuth with the intercalated lithium.

$\text{Li}^+$  and  $\text{Na}^+$  with estimated bismuth contact distances of 176, 205, and 241 pm, respectively. The channels are probably too small for  $\text{Ag}^+$ . In the following, we choose  $\text{Li}^+$  as a representative intercalate, one of much interest and application in technology,<sup>28,29</sup> and analyze its interaction upon intercalation into the bismuth channels to form  $\text{Li}^+_x\text{-Ti}_4\text{FeBi}_2$ . In order to maintain the full translational symmetry in our calculation we choose  $x = 1$ , which implies occupation of all the quasi-tetrahedral holes. This leads to an appropriate description of the interaction of the  $\text{Li}^+$  guest cation with the  $\text{Ti}_4\text{FeBi}_2$  host. However, in real systems the occupation number will be much lower and governed by defects in the host which allow for the charge compensation. For  $x = 1$ , i.e., on completely filling the channels with  $\text{Li}^+$ , the structure of the  $\text{Li}^+_1\text{-Ti}_4\text{FeBi}_2$  intercalation compound is closely related to  $\text{W}_5\text{Si}_3$  in the notation  $\text{W1-W}_2\text{Si}_2$ , where W1 and W2 represent the two inequivalent tungsten positions. However, the slightly different positional

parameters and the substitution of silicon with bismuth lead to a quite distinct atomic environment of W1 and  $\text{Li}^+$  in the respective compounds.

In Figure 11 we give the lithium contribution to the DOS for  $\text{Li}^+_1\text{-Ti}_4\text{FeBi}_2$  (left panel) and the Bi-Li crystal orbital overlap population (right panel), from which we find all-bonding bismuth-lithium interaction from the bottom of the valence band up to the Fermi level at  $-6.5$  eV. Electron redistribution from bismuth and titanium to lithium leads to electron accumulation on the alkali metal, which becomes pretty negatively charged ( $-1.3e$ ). Comparing the DOS of the host (Figure 2) with the DOS of the intercalation compound, we find for the latter case a stabilization and broadening of the mainly Bi(6s)-derived energy levels below  $-15$  eV, which is caused by Bi(6s)-Li(2s) and Bi(6s)-Li(2p) bonding interactions. The corresponding antibonding states lie in the energy region starting just after the gap at  $-11.8$  eV and overlapping with the Bi-

(28) Owen, J. R. *Chem. Soc. Rev.* **1997**, 26, 259.

(29) Pistoia, G., Ed. *Lithium Batteries*; Elsevier: Amsterdam, 1994.



**Table 2.** Extended Hückel Parameters

element	AO	$H_{ii}/eV$	$\zeta_1$	$\zeta_2$	$c_1$	$c_2$
Ti	4s	-6.30	1.500			
	4p	-3.20	1.500			
	3d	-5.90	4.550	1.400	0.4206	0.7839
Mn	4s	-7.50	1.800			
	4p	-3.80	1.800			
	3d	-8.70	5.150	1.700	0.5140	0.6930
Fe	4s	-7.60	1.900			
	4p	-3.80	1.900			
	3d	-9.20	5.350	1.800	0.5366	0.6678
Co	4s	-7.80	2.000			
	4p	-3.80	2.000			
	3d	-9.70	5.550	1.900	0.5550	0.6678
Ni	4s	-7.80	2.100			
	4p	-3.70	2.100			
	3d	-9.90	5.750	2.000	0.5683	0.6292
Bi	6s	-15.19	2.560			
	6p	-7.79	2.072			
Li	2s	-9.0	0.703			
	2p	-8.0	0.703			

(6p)–Li(2s) and Bi(6p)–Li(2p) bonding states. Thus they are not easily seen in the Bi–Li COOP curve.

On moving the  $Li^+$  from the center of the imperfect tetrahedron to halfway between two Bi atoms (at the middle point of the tetrahedral edge), we found an approximately 4 eV (1 eV per  $Li^+$ ) increase in the electronic energy. This suggests that  $Li^+$  prefers to occupy the quasi-tetrahedral sites; the calculated barrier to motion through the channel is probably not reliably given by the extended Hückel calculation.

## Conclusion

We have analyzed the electronic structure and chemical bonding in the ternary transition metal bismuthides  $Ti_4TBi_2$  with  $T = Cr, Mn, Fe, Co,$  and  $Ni$ . These intermetallic compounds feature strong Ti– $T$  and Ti–Bi bonds. The titanium–bismuth sublattice plays an important role in determining the short  $T$ – $T$  distances, whose decrease along the series is enhanced by titanium–titanium and titanium–bismuth interlayer interactions. The shortening of the titanium–titanium bonds is due to titanium d–d bonding which is strengthened by an increasing electron filling of the titanium d levels along the transition metal series. The titanium–bismuth interactions remain strong from  $Ti_4CrBi_2$  to  $Ti_4NiBi_2$ ; this can also be seen from the (almost) constant *intralayer* titanium–bismuth distances.

We have shown that the empty bismuth channels are filled with essentially unhybridized Bi(6p) orbitals, which form a two-

dimensional net in the *ab* plane, stacking along *c*, and interacting with each other—stronger along than across the channels. Overlap of these 6p orbitals within the  $Ti_4Bi_2$  octahedra provides electronic communication between the bismuth channels perpendicular to the *c* direction.

The (imperfect) tetrahedral holes in the bismuth channels are big enough to incorporate  $H^+$ , or the alkali metal cations  $Li^+$  and  $Na^+$ . A study of the hypothetical intercalation of  $Li^+$ , which is of great interest in view of technological applications, finds much bismuth–lithium interaction from the bottom of the valence band up to the Fermi level.

**Acknowledgment.** We thank Y. Wang and E. Merschrod for stimulating discussions and three reviewers for a careful reading of this paper. R.R. acknowledges the Schweizerischer Nationalfonds zur Förderung der wissenschaftlichen Forschung for a postdoctoral fellowship. Our work at Cornell was supported by the National Science Foundation through Research Grant CHE-94-08455.

## Appendix

Extended Hückel tight-binding (EHTB) calculations<sup>7,8</sup> were carried out with the YAeHMOP program package.<sup>30</sup> Standard parameters (listed in Table 2) were used, and the tetragonal Brillouin zone was sampled at 27 *k* points in reciprocal space.<sup>31</sup> Calculations with more *k* points yielded the same results. Density of states (DOS) and crystal orbital overlap population (COOP) curves were obtained by fitting Gaussian lobes of half widths 0.025 (eV) at 2000 data points in the energy range from –18 to 2 eV (energy step 0.01 eV) to the respective discrete values and summing up their contributions. The input geometries were generated with the CACHe Editor<sup>32</sup> based on the atomic parameters determined from single-crystal X-ray spectrometry.<sup>1</sup>

The local geometry of the  $BiH_3$  molecules is  $91^\circ$  for the H–Bi–H angles and 181 pm for the Bi–H bond lengths, as given in ref 33 and shown in Figure 7.

IC981075V

(30) Landrum, G. A. *YAeHMOP, Yet Another extended Hückel Molecular Orbital Package*; YAeHMOP is freely available on the World Wide Web at the URL <http://overlap.chem.cornell.edu:8080/yaehmop.html>, 1997.

(31) Ramírez, R.; Böhm, M. C. *Int. J. Quantum Chem.* **1986**, *30*, 391.

(32) *CACHe Editor*; CACHe Scientific, Inc.: Oxford, U.K., 1994.

(33) Schwerdtfeger, P.; Laakkonen, L. J.; Pyykkö, P. *J. Chem. Phys.* **1992**, *96* (9), 6807.